International Journal of Engineering

Journal Homepage: www.ije.ir

Formation Control and Obstacle Avoidance of a Multi-Quadrotor System Based on Model Predictive Control and Improved Artificial Potential Field

F. Ghaderi[a], A. Toloei[*a], R. Ghasemi[b]

[a] *Department of Aerospace Engineering, Shahid Beheshti University, Tehran, Iran*
[b] *Department of Engineering, University of Qom, Qom, Iran*

P A P E R I N F O

Paper history:
Paper history: Received 16 June 2023
Received in revised form 18 July 2023
Accepted 19 July 2023

Keywords:
Quadrotor
Formation Control
Model Predictive Control
Obstacle Avoidance
Improved Artificial Potential Field

A B S T R A C T

The purpose of this article is to control the formation and pass static and dynamic obstacles for the quadrotor group, maintain the continuity and flight formation after crossing the obstacles, and track the moving target. Model Predictive Control (MPC) method has been used to control the status and position of quadrotors and formation control. Flight formation is based on the leader-follower method, in which the followers maintain a certain angle and distance from the leader using the formation controller. The improved Artificial Potential Field (APF) method has been used to pass obstacles, the main advantage of which compared to the traditional APF is to increase the range of the repulsive force of the obstacles, which solves the problem of getting stuck in the local minimum and not passing through the environments full of obstacles. The results of the design of the attitude and position controller showed that the quadrotors were stabilized and converged in less than 3 seconds. Formation control simulations in the spiral path showed that the followers, follow the leader. The results of the quadrotors passing through the obstacles were presented in four missions. In the first mission, 4 quadrotors crossed static obstacles. In the second mission, 4 quadrotors crossed dynamic obstacles. In these two missions, the quadrotors maintained a square flight formation after crossing the obstacles. In the third mission, the number of quadrotors increased to 6. The leader tracked the moving target and the quadrotors crossing the static obstacles. In the last mission, the quadrotors passed through the dynamic obstacles and the leader tracked the static target. In these missions, the quadrotors maintain the hexagonal formation after crossing the obstacles. The results simulations showed that the quadrotors crossed the fixed and moving obstacles and after crossing, they preserved the flight formation.

***doi**: 10.5829/ije.2024.37.01a.11*

1. INTRODUCTION

Robots have been widely used in military and civilian fields such as anti-terrorism operations, identification, agriculture, etc. (1, 2). In addition, instead of using a single robot, multiple robots in a group formation can complete some complex missions without incurring high costs (3, 4). Among the controllers used to control the formation is model predictive control (MPC). MPC is a controller where optimization is solved online. The vital advantage of this method is considering a performance criterion and constraints. For multi-agent systems, the time of optimization calculations increases with the number of agents. To solve this problem, decentralized MPC (5, 6) or distributed MPC (7) have been proposed. The formation control of multiple robots is generally classified into leaderless and leader-follower (8). In the leaderless formation control problem, the robots are driven to a prescribed pattern at a certain speed. In contrast in the leader-follower control problem, the follower robots agree on the reference information of a leader while maintaining the defined pattern. In the control of leader-follower formation, the problem of the availability of information about the leader can be solved by distributed technique. A distributed control approach was designed by Zou and Meng (8) by introducing

*Corresponding Author Institutional Email: toloei@sbu.ac.ir
(A. Toloei)

Please cite this article as: Ghaderi F, Toloei A, Ghasemi R. Formation Control and Obstacle Avoidance of a Multi-Quadrotor System Based on Model Predictive Control and Improved Artificial Potential Field. International Journal of Engineering, Transactions A: Basics. 2024;37(01): 115-126.

distributed estimators to obtain reference information for leader-follower control. Another distributed control algorithm was proposed by Dong et al. (9) to track the flight formation of multiple robot leader-follower. In addition, a non-smooth distributed control algorithm was developed by Du et al. (10), so that the robot leader-follower control tracking was achieved. In addition, with the help of a sub-optimal H∞ strategy, a distributed leader-follower control algorithm is designed by Jasim et al. (11) that is robust to disturbances and parameter uncertainties. Although the control schemes proposed in the mentioned papers are convincing in hierarchical leader-follower formation control tracking, the control command extraction may cause singularities and chattering, which may cause implementation problems in practical applications. Also, in these articles, the flight group has a flight arrangement in a simple route, and the issue of moving target tracking has not been investigated. In this article, the MPC method is used for formation control in which there is no possibility of chattering, and the flight path is a spiral path, and the issue of moving target tracking is also investigated.

It is essential, to maintain the safety of the operations in the missions that the UAV group performs. One of the most important safety issues is avoiding obstacles. If a group of quadrotors encounters obstacles in an unknown environment, each drone must recognize the obstacle and pass through it. Crossing obstacles is necessary to avoid accidents and make the flight safe. This article focuses on the crossing of the quadrotor group through static and dynamic obstacles and maintaining the flight arrangement after crossing the obstacles. The methods of solving the collision avoidance problem are different for dynamic and static obstacles. A* (12), Genetic (13), Differential Evolution (14), Ant Colony Optimization (15), and Particle Swarm Optimization (16) methods are usually used to avoid static obstacles. Methods for dealing with dynamic obstacles include Fuzzy Logic Algorithm (17), Neural Network (18), Rapidly-exploring Random Trees (19), and APF (20). Shang et al. (21) used the terminal nonsingular sliding mode controller for the problem of control formation and obstacle avoidance. Quadrotors have maintained formation flight after crossing obstacles. In this paper, only static obstacles are considered.

One of the most widely used methods to identify and avoid obstacles is the APF method. Which is expressed by mathematical equations and has advantages such as high safety and simplicity of calculations. In this method, a positive potential field is considered for obstacles, and a negative potential field for the target. The drone is attracted to the target by avoiding obstacles. Pan et al. (22) introduced formation control which is based on the leader-follower method, in which the PD is used to control the position and attitude of the quadrotors, and the APF is used to pass the obstacles. To prove the effectiveness of the above method, several experiments have been performed. In this article, crossing dynamic obstacles is not investigated. Wang and Zhang (23) have presented a rapidly-exploring random trees algorithm for the formation control and crossing obstacles, in which the lack of vigilance and low speed of the APF method is compensated by the sampling method. In this article, crossing static obstacles is considered. Qiao et al. (24) have provided formation control based on distributed control. The potential function is used to avoid the collision. A virtual navigator determines the movement of agents. In this article, the obstacles are static, and the drones maintain the connection after crossing. Aljassani et al. (25) presented a new APF method for the UAV group to pass through obstacles, which solves the problem of getting stuck in a local minimum. The leader-follower method is used for group movement. The obstacles considered are two static obstacles. In these articles, the crossing of dynamic obstacles is not investigated. Huang et al. (26) have investigated dynamic obstacles avoidance and maintaining continuity and formation flight after crossing obstacles. The sliding mode method and the virtual potential field method are used for control formation and obstacle avoidance. Zhang et al. (27) proposed a distributed control method for quadrotor group flight formation. The disadvantages of this method are getting stuck in a local minimum and unreachable goals in environments full of obstacles (28). To solve these problems, some approaches have been proposed. Methods are also proposed for broader problems, such as dynamic obstacle avoidance or integration of UAV kinematic models to improve tracking accuracy (29, 30). In the mentioned articles, simultaneously crossing the dynamic and static obstacles and maintaining the flight formation after crossing the obstacles and tracking the mobility target simultaneously have not been discussed and, in a small number of these articles, the improvement of the potential field method has been investigated to solve its problems.

The necessity of doing this article is to improve the potential field method for the passage of the flight group through dynamic obstacles and maintain the connection between the agents.

The innovation of this paper is that it presented an improved potential field method for crossing static and dynamic obstacles and maintaining continuity after crossing obstacles. Where instead of considering a circular repulsion field for obstacles, an elliptical field is considered, which causes the repulsion range of obstacles to be greater and, as a result, solves the problem of getting stuck in the local minimum and not reaching the target in obstacle-filled environments to a great extent, and simultaneously, the leader tracks the moving target while maintaining the flight formation.

The article's structure is as follows: In the first section, the dynamic modeling of the quadrotor is

presented. The following section deals with attitude and position controllers. In the third section, the control formation is given; in the fourth section, the crossing of obstacles is discussed; and in the last section, the results are presented.

2. DYNAMIC MODEL OF QUADROTOR

The six degrees of freedom model is obtained according to the Newton-Euler method. Total rotors velocity and the rotor velocity vector are as follows:

$$\Pi == +\varpi_4 + \varpi_2 - \varpi_1 - \varpi_3 \quad , \quad \Pi = \begin{bmatrix} \varpi_1 \\ \varpi_2 \\ \varpi_3 \\ \varpi_4 \end{bmatrix} \tag{1}$$

where $(\varpi_1, \varpi_2, \varpi_3, \varpi_4)$ show the speeds of the rotors. The effect of the motion vector on the quadrotor dynamics is given below:

$$U_B(\varpi) = E_B \varpi^2 = \begin{bmatrix} 0 \\ 0 \\ U_1 \\ U_2 \\ U_3 \\ U_4 \end{bmatrix} = \begin{bmatrix} 0 \\ 0 \\ b(\varpi_1^2 + \varpi_2^2 + \varpi_3^2 + \varpi_4^2) \\ bl(\varpi_4^2 - \varpi_2^2) \\ bl(\varpi_3^2 - \varpi_1^2) \\ c_d(\varpi_2^2 + \varpi_4^2 - \varpi_1^2 - \varpi_3^2) \end{bmatrix} \tag{2}$$

where, l is the length from the center of mass to each rotor, c_T is the thrust force coefficient, and c_d is the drag force coefficient. The E_B and $U_B(\varpi)$, which show the motion matrix and the motion vector, are as follows.

$$E_B = \begin{bmatrix} 0 & 0 & 0 & 0 \\ 0 & 0 & 0 & 0 \\ c_T & c_T & c_T & c_T \\ 0 & -c_T l & 0 & c_T l \\ -c_T l & 0 & c_T l & 0 \\ -c_d & c_d & -c_d & c_d \end{bmatrix} \tag{3}$$

The dynamical equations of the quadrotor are given below:

$$\dot{\vartheta}_1 = \dot{\phi} = \ddot{\phi} + \ddot{\theta} sin\phi tan\theta + \ddot{\psi} cos\,\phi tan\theta$$

$$\dot{\vartheta}_2 = \dot{\theta} = \ddot{\theta} cos\phi - \ddot{\psi} sin\,\phi$$

$$\dot{\vartheta}_3 = \dot{\psi} = \frac{sin\phi}{cos\theta}\ddot{\theta} + \frac{cos\phi}{cos\theta}\ddot{\psi}$$

$$\dot{\vartheta}_4 = \dot{x} = \vartheta$$

$$\dot{\vartheta}_5 = \dot{y} = \vartheta$$

$$\dot{\vartheta}_6 = \dot{z} = \vartheta$$

$$\dot{\vartheta}_7 = \dot{P} = \frac{I_{YY} - I_{ZZ}}{I_{XX}} RQ - \frac{J_{Tp}}{I_{XX}} Q\,\Omega + \frac{U_2}{I_{XX}}$$

$$\dot{\vartheta}_8 = \dot{Q} = \frac{I_{ZZ} - I_{XX}}{I_{YY}} RP + \frac{J_{Tp}}{I_{YY}} P\,\Omega + \frac{U_3}{I_{YY}}$$

$$\dot{\vartheta}_9 = \dot{R} = \frac{I_{XX} - I_{YY}}{I_{ZZ}} PQ + \frac{U_4}{I_{ZZ}}$$

$$\begin{aligned} \dot{\vartheta}_{10} &= \dot{U} = (-WQ + VR) + g s_\theta \\ \dot{\vartheta}_{11} &= \dot{V} = (-UR + WP) - g c_\theta s_\phi \\ \dot{\vartheta}_{12} &= \dot{W} = (-UQ + VP) - g c_\theta s_\phi + \frac{U_1}{m} \end{aligned} \tag{4}$$

where, J_{Tp} is the moment of total rotation of inertia about the rotor axis, (U, V, W) are the linear velocities, (P, Q, R) are roll, pitch, and yaw, and I_{XX}, I_{YY}, and I_{ZZ} are the moments of inertia in the x, y, and z-axis, whose values are given in Table 1. the rotors speed inputs U_1, U_2, U_3, and U_4 are as follows (21):

$$\begin{aligned} U_1 &= c_T(\varpi_1^2 + \varpi_2^2 + \varpi_3^2 + \varpi_4^2) \\ U_2 &= l c_T\,(-\varpi_2^2 + \varpi_4^2\,) \\ U_3 &= l\; c_T\,(-\varpi_1^2 + \varpi_3^2\,) \\ U_4 &= c_d(-\varpi_1^2 + \varpi_2^2 - \varpi_3^2 + \varpi_4^2) \\ \varpi &= -\varpi_1 + \varpi_2 - \varpi_3 + \varpi_4 \end{aligned} \tag{5}$$

3. MPC CONTROLLER

The predictive controller is used in the industry because of its advantages, such as dealing with disturbances, limitations and uncertainties. In this article, a generalized predictive controller is used, which has features such as dealing with non-minimum phase systems and having additional control horizon parameters. In this controller, the control signal is obtained by minimizing the multi-step function in the prediction horizon. As a result, according to the integral behavior in the state space, it is possible to replace $u(k)$ with $\Delta u(k) = u(k) - u(k-1)$ in the equations. The state space equations are given below:

$$\begin{bmatrix} \Delta x_m(k+1) \\ y(k+1) \end{bmatrix} = \begin{bmatrix} A_m & 0_{q\times n}^T \\ C_m A_m & I_{q\times q} \end{bmatrix} \begin{bmatrix} \Delta x_m(k) \\ y(k) \end{bmatrix} + \begin{bmatrix} B_m \\ C_m B_m \end{bmatrix} \Delta u_m(k) + \begin{bmatrix} B_d \\ C_m B_m \end{bmatrix} \varepsilon(k)$$

$$y(k) = \begin{bmatrix} 0_{q\times n}^T & I_{q\times q} \end{bmatrix} \begin{bmatrix} \Delta x_m(k) \\ y(k) \end{bmatrix} \tag{6}$$

TABLE 1. Parameters of quadrotor dynamic

Parameter	Value
I_{XX}	$\mathbf{11 \times 10^{-2}\ kg\ m^2}$
I_{YY}	$\mathbf{19 \times 10^{-2}\ kg\ m^2}$
I_{ZZ}	$\mathbf{1.3 \times 10^{-2}\ kg\ m^2}$
J_{Tp}	$\mathbf{6 \times 10^{-5}\ kg\ m^2}$
m	$\mathbf{3.23\ kg}$
l	$\mathbf{0.23\ m}$
c_d	$\mathbf{7.5 \times 10^{-7}\ N\ m\ s^2}$
c_T	$\mathbf{3.13 \times 10^{-5}\ N\ s^2}$

The output is defined as below:

$$Y = H'x(k) + H".\Delta U \tag{7}$$

where:

$$H' = \begin{bmatrix} CA \\ CA^2 \\ CA^3 \\ \vdots \\ CA^{N_p} \end{bmatrix}, H" = \begin{bmatrix} CB & 0 & 0 & \dots & 0 \\ CAB & CA & 0 & \dots & 0 \\ CA^2B & CAB & CB & \dots & 0 \\ \vdots & \vdots & \vdots & \ddots & \vdots \\ CA^{N_p-1}B & CA^{N_p-2}B & CA^{N_p-3}B & \dots & CA^{N_p-N_c}B \end{bmatrix} \tag{8}$$

The cost function is considered as below:

$$J = (Y-w)^T W_y (Y-w) + \Delta U^T W_u \Delta U \tag{9}$$

where, Y is the vector of predicted outputs, w is the vector of reference signal values in future times, ΔU is the control signal, and W_u and W_y define the weight of inputs and outputs in the cost function.

The necessary condition for minimizing the cost function is given below:

$$\frac{\partial J}{\partial \Delta U} = 0$$

By satisfying the above condition, u is obtained as follows (31):

$$\Delta U = (H^{"T} W_y H^{"} + W_u)^{-1} H^{"T} W_y (w - H'x(k)) \tag{10}$$

4. FORMATION FLIGHT

Formation control patterns include virtual structure and behavior-based, and leader-follower. In the virtual structure method, each agent is considered an element of a larger structure. In this method, all the arrangement members act as a single rigid body and follow a determined path. This method is suggested to maintain formation while moving. As a result, this method is unsuitable for crossing a group of obstacles because it is necessary to change the formation to pass the obstacles. In addition to the group movement, searching and reaching the desired target is also investigated in the behavior-based structure. The weakness of this method is the difficulty of analyzing the overall behavior of the formation and its mathematical analysis and checking its stability.

In the leader-follower algorithm, one or more agents are designated as leaders, and other quadrotors are considered followers, so the followers must follow the leader with a fixed direction and position. The control of the formation of multi-agent systems using the leader-follower structure has received special attention due to its simplicity and scalability. Since the movement of other vehicles in the formation is completely determined by the leading position, the leading position creates coordination. Therefore, the followers follow the leader to maintain the formation. The advantage of this method is that it is easy to understand and more practical in implementation .This model is used in this article.

4. 1. Formation Control In this article, quadrotor group control formation and obstacle avoidance are investigated. Formation flight is controlled by the MPC method. The pattern used is leader-follower. In the leader-follower method, the leader follows a determined path, and the followers maintain a certain angle and distance from the leader. Figure 1 illustrates this method. In this figure, λ is the distance from the center of the leader mass to the center of the follower mass, and φ is the angle between the x-axis and λ line.

$$\begin{cases} \lambda_x = -(x_L - x_F)\cos\psi_L - (y_L - y_F)\sin\psi_L \\ \lambda_y = -(x_L - x_F)\sin\psi_L - (y_L - y_F)\cos\psi_L \end{cases} \tag{11}$$

$$\begin{aligned} \lambda_x^d &= \lambda\cos\varphi \\ \lambda_y^d &= \lambda\sin\varphi \end{aligned} \tag{12}$$

The formation error is given below:

$$\begin{cases} e_x = \lambda_x^d - \lambda_x \\ e_y = \lambda_y^d - \lambda_y \\ e_\psi = \psi_F - \psi_L \end{cases}$$

$$\begin{cases} \dot{e}_x = \dot{\lambda}_x^d - \dot{\lambda}_x \\ \dot{e}_y = \dot{\lambda}_y^d - \dot{\lambda}_y \\ \dot{e}_\psi = \dot{\psi}_F - \dot{\psi}_L \end{cases} \tag{13}$$

λ^d and φ^d are constant parameters, therefore, λ_x^d and λ_y^d have constant values and, their derivatives $\dot{\lambda}_x^d$ and $\dot{\lambda}_y^d$ are zero. The transition dynamics on the x-y plane are present below:

$$\begin{cases} \dot{x}_i = v_{ix}\cos\psi_i - v_{iy}\sin\psi_i \\ \dot{y}_i = v_{ix}\sin\psi_i + v_{iy}\cos\psi_i \\ \dot{\psi}_L = \omega_L \end{cases} \tag{14}$$

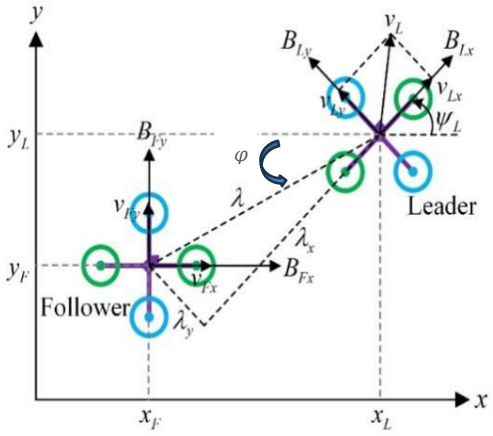

Figure 1. Quadrotor formation in x-y plane

i indicate leader (i = L) or follower (i = F) . $\dot{x}_i$ and $\dot{y}_i$ are velocities in the ground coordinate system. ψ_i is the angle between the x-axis of the body and the ground coordinate system, and v_{ix} and v_{iy} are the velocities in the body coordinate system:

$$\begin{cases} v_{ix} = \dot{x}_i \cos\psi_i + \dot{y}_i \sin\psi_i \\ v_{iy} = -\dot{x}_i \sin\psi_i + \dot{y}_i \cos\psi_i \end{cases} \quad (15)$$

As a result, the following relations are obtained.

$$\begin{cases} \dot{e}_x = -(\lambda_y^d - e_y)\omega_L - v_{Fx}\cos e_\psi + v_{Fy}\sin e_\psi + v_{Lx} \\ \dot{e}_y = (\lambda_x^d - e_x)\omega_L - v_{Fx}\sin e_\psi - v_{Fy}\cos e_\psi + v_{Ly} \\ \dot{e}_\psi = \omega_F - \omega_L \end{cases} \quad (16)$$

The state space is as below.

$$\dot{x} = A(x) + B(x)\tau \quad (17)$$

where x is the state vector and τ is the control input, and M(x) and N(x) are defined as follows (32):

$$x = [e_x \quad e_y \quad e_\psi]^T \quad (18)$$

$$\tau = [\tau_{Fx} \quad \tau_{Fy} \quad \omega_F]^T \quad (19)$$

$$A(x) = \begin{bmatrix} e_y\omega_L + \tau_{Lx} - \omega_L\lambda_y^d \\ -e_x\omega_L + \tau_{Ly} + \omega_L\lambda_x^d \\ -\omega_L \end{bmatrix} \quad (20)$$

$$B(x) = \begin{bmatrix} -\cos e_\psi & \sin e_\psi & 0 \\ -\sin e_\psi & -\cos e_\psi & 0 \\ 0 & 0 & 1 \end{bmatrix} \quad (21)$$

The control law for the formation of the quadrotors based on MPC (33) is considered as follows:

$$\begin{aligned} & M_i(k) = -\sum_{j=1}^{N+1} a_{ij}\left[\sum_{k=0}^{3}\beta_k\left(f_i^{(k)} - \hat{f}_j^{(k)}\right)\right], \\ & i\epsilon\{1,2,\dots.,N\}, \\ & \hat{f}_j^{(k)} = f_j^{(k)} - d_{fj}^{(k)}, \quad j\epsilon\{1,2,\dots.,N+1\}, \\ & \begin{cases} \beta > 0 \ \forall k\epsilon\{0,1,2,3\} \\ \lambda_{min} > \frac{\beta_1^2}{\beta_1\beta_2\beta_3 - \beta_0\beta_3^2} \\ \beta_1\beta_2 > \beta_0\beta_3 \end{cases} \end{aligned} \quad (22)$$

where i and $N + 1$ represent quadrotor i and the leader. The control gains $\beta_k\epsilon\mathbb{R}, k\epsilon\{0,1,2,3\}$ must satisfy conditions (13). $d_{fj}^{(k)}\boldsymbol{\epsilon}\mathbb{R}^{\mathbf{2}}$ is the desired state between $quadrotor\ j$ and the leader on the horizontal plane. The control law for the formation flight of $quadrotor\ i$ in the vertical direction (34) is as follows:

$$\begin{aligned} & T_i(k) = -\sum_{j=1}^{N+1} a_{ij}\left[\sum_{k=0}^{3}\gamma_k\left(h_i^{(k)} - \hat{h}_j^{(k)}\right)\right], \\ & i\epsilon\{1,2,\dots.,N\}, \\ & \hat{h}_j^{(k)} = h_j^{(k)} - d_{hj}^{(k)}, \quad j\epsilon\{1,2,\dots.,N+1\}, \\ & k\epsilon\{0,1\}, \\ & \gamma_k > 0, \ k\epsilon\{0,1\}, \end{aligned} \quad (23)$$

where $\gamma_k\epsilon\mathbb{R}\ k\epsilon\{0,1\}$ is control gains and $d_{hj}^{(k)}\epsilon\mathbb{R}^2$ is the desired relative state between $quadrotor\ j$ and the leader in the vertical direction.

5. IMPROVED ARTIFICIAL POTENITIAL FIELD

In the APF, attractive potential is considered for the target, and repulsive potential is considered for the obstacles. The agent moves away from the obstacles by moving towards the target.

The control of the agent by the AFP is as below:

$$U_{ar}(x) = U_a(x) + U_r(x) \quad (24)$$

where, $U_{ar}, U_a, and\ U_r,$ represent the potential of attraction, the potential of repulsion, and the potential virtual field. Gradient functions are stated as follows:

$$\begin{aligned} & F_{art} = F_a + F_r \\ & F_a = -grad[U_a(x)] \\ & F_r = -grad[U_r(x)] \end{aligned} \quad (25)$$

where $\boldsymbol{F_a}$ is the robot's attraction, and $\boldsymbol{F_r}$ is the force created by $\boldsymbol{U_r(x)}$. The attraction coefficient $\boldsymbol{k_a}$ and the potential attraction field $\boldsymbol{U_a(x)}$ are given below:

$$U_a = \frac{1}{2}k_a R_a^2 \quad (26)$$

The $\boldsymbol{U_r}$ (x) is as follows:

$$U_r(x) = \begin{cases} 0.5k_a(\frac{1}{R_r} - \frac{1}{X_0})^2 & R_r \le X_0 \\ 0 & R_r > X \end{cases} \quad (27)$$

where $\boldsymbol{X_0}$ is the safe distance from the obstacles.

$\boldsymbol{R_a = \|X_d - X\| = \sqrt{(x - x_d)^2 - (z - z_d)^2 - (y - y_d)^2}}$ is the distance from the agent to the target, $\boldsymbol{R_r = \|X_u - X\| = \sqrt{-(z - z_u)^2 + (x - x_u)^2 - (y - y_u)^2}}$ is the shortest distance from the agent, and the obstacles, where $\mathbf{X} = (\mathbf{x}, \mathbf{y}, \mathbf{z})$, $\boldsymbol{X_m} = (\boldsymbol{x_m}, \boldsymbol{y_m}, \boldsymbol{z_m})$, and $\boldsymbol{X_d} = (\boldsymbol{x_d}, \boldsymbol{y_d}, \boldsymbol{z_d})$ are the position of the agent, the position of obstacles and the position of the target. The functions of repulsion and attraction are present below:

$$\begin{aligned} & F_a = -\nabla\left(\frac{1}{2}k_a R_a^2\right) k_a R_a \\ & U_r(x) = \begin{cases} k_a(\frac{1}{R_r} - \frac{1}{R_r{}^2})\frac{1}{R_r{}^2} & R_r \le X_0 \\ 0 & R_r > X_0 \end{cases} \end{aligned} \quad (28)$$

The traditional APF method works poorly in obstacle environments, and may get stuck in a local minimum. To solve this issue, the improved APF is used. The spherical repulsion field has been changed to an elliptic field in the APF. According to Figure 2, the agent is placed in the

center of the ellipse and the locations of the obstacles are C and D. Around the agent, there is an ellipse repulsion field, and the obstacles are placed on the edges of the ellipse, which have different distances from the agent. As a result, the repulsive field created can repel obstacles more effectively (The range of repulsive increases). The advantage of this way is that it allows a greater safety distance for the agent to pass and makes it easier to pass obstacles in complex environments. The parameters of the ellipsoidal APF are proportional to the velocity of the agent. The magnitudes of its long semi-axis $\boldsymbol{a}$ and middle semi-axis $\boldsymbol{b}$ are determined by the components of the agent's velocity. The focal length is $\boldsymbol{c_1 = \sqrt{\alpha^2 - \beta^2}}$, and combined with the agent's coordinates and the velocity direction can be derived from the coordinates of the two focal points of the ellipse, as follows:

$$\begin{aligned}
&\boldsymbol{x_{c1} - x_m = -\varrho v_x}\\
&\boldsymbol{y_{c1} - y_m = -\varrho v_y}\\
&\boldsymbol{z_{c1} - z_m = -\varrho v_z}\\
&\boldsymbol{(x_{c1} - x_m)^2 + (y_{c1} - y_m)^2 + (z_{c1} - z_m)^2 = \alpha^2 - \beta^2}\\
&\boldsymbol{x_{c2} - x_m = -\varrho v_x}\\
&\boldsymbol{y_{c2} - y_m = -\varrho v_y}\\
&\boldsymbol{z_{c2} - z_m = -\varrho v_z}\\
&(x_{c2} - x_m)^2 + (y_{c2} - y_m)^2 + (z_{c2} - z_m)^2 = \alpha^2 - \beta^2
\end{aligned} \tag{29}$$

where $\boldsymbol{(x_m, y_m, z_m)}$, $\boldsymbol{(x_{H1}, y_{H1}, z_{H1})}$, and $\boldsymbol{(x_{H2}, y_{H2}, z_{H2})}$ are the coordinates of the robot and focal $\boldsymbol{H_1}$, $\boldsymbol{H_2}$ of the ellipse. The condition for determining the presence of obstacles in the improved APF requires the geometric definition of an ellipse and the sum of the distances from the obstacles to the two focal points of the ellipse are:

$$\begin{aligned}
&d^1, A, H_1, H_2 =\\
&\sqrt{(x - x_{H1})^2 + (y - y_{H1})^2 + (z - z_{H1})^2} +\\
&\sqrt{(x - x_{H2})^2 + (y - y_{H2})^2 + (z - z_{H2})^2}
\end{aligned} \tag{30}$$

The mentioned equation can be approximated as follows:

$$d, A, H_1, H_2 = d^1, A, H_1, H_2 - 2X_0 \tag{31}$$

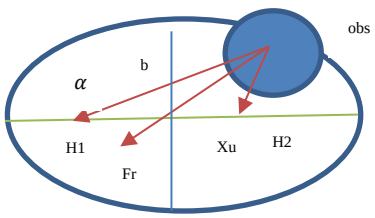

Figure 2. Diagram of the APF with elliptical cross-section

If $\boldsymbol{A, H_1, H_2 \le 2\alpha}$ The obstacle will probably collide with the agent and needs a way to avoid the collision. If $\boldsymbol{A, H_1, H_2 > 2\alpha}$ there is no possibility of collision. For ease of calculations, the repulsive function of the improved APF is considered as below:

$$U_r = \begin{cases} \frac{1}{2} k_a \left(\frac{1}{d, A, H_1, H_2 - 2\alpha} - \frac{1}{X_0}\right)^2, & A, H_1, H_2 \le 2\alpha \\ 0, & A, H_1, H_2 > 2\alpha \end{cases} \tag{32}$$

The repulsive force on the agent is given below:

$$F_r = -\Delta U_r = \begin{cases} k_a \left(\frac{1}{d, A, H_1, H_2 - 2\alpha} - \frac{1}{X_0}\right) \frac{1}{d^2 A, H_1, H_2}, d & A, H_1, H_2 \le 2\alpha \\ 0, & A, H_1, H_2 > 2\alpha \end{cases} \tag{33}$$

where $\boldsymbol{d\,x, x_{H1}, x_{H1} \le 2\alpha}$ indicates the repulsive force that acts within the ellipsoid. The total force on the agent is as below:

$$F_{total}(x) = \sqrt{(F_{ax} + F_{rx})^2 + (F_{ay} + F_{ry})^2 + (F_{az} + F_{rz})^2} \tag{34}$$

5. SIMULATIONS AND RESULTS

In this section, the results of obstacle avoidance using the improved APF for a group of quadrotors (Figure 3) in 4 missions are present. First, the simulation results of quadrotor attitude and position control are presented by the MPC method.

Figure 4 shows the attitude of the quadrotor controlled using the MPC method. Severe overshoot and undershoot are not seen in the responses. The convergence time of (ϕ, θ, ψ) are $(1, 0.9, 2)$ seconds.

Figure 5 shows the position of the robot. According to this figure, the responses track the reference well and converge in less than 1 second.

In the following, the simulation results of the control formation are presented.

Figure 6 indicates the position of robots in the S-shaped path in which five follower quadrotors follow the leader.

Figure 7 indicates the attitude of quadrotors in the S-shaped path in which five follower quadrotors follow the leader well. The maximum convergence time of the follower's attitude (ϕ, θ, ψ) is (6s,6s,9s).

Figure 8 presents the position of agents in 3D space, where followers follow the leader in the S-shaped path.

The results of the formation flight simulation are more than 90% consistent with the reported data in literature (32, 35).

The results of avoiding collision with obstacles using the improved APF are given in 3 missions. In the first mission, the quadrotors have a square formation that

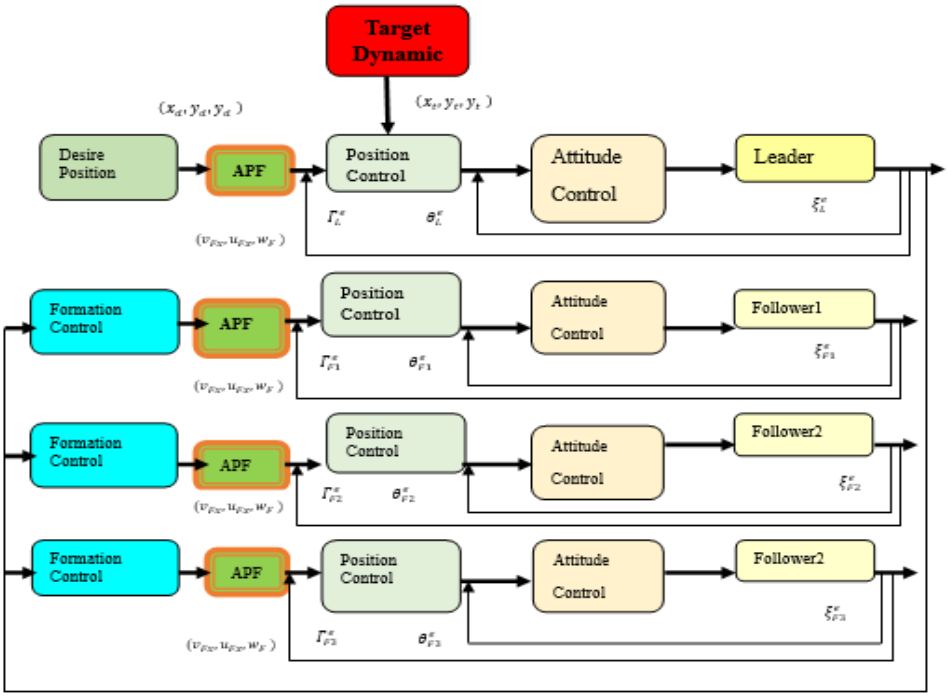

Figure 3. Formation control block diagram

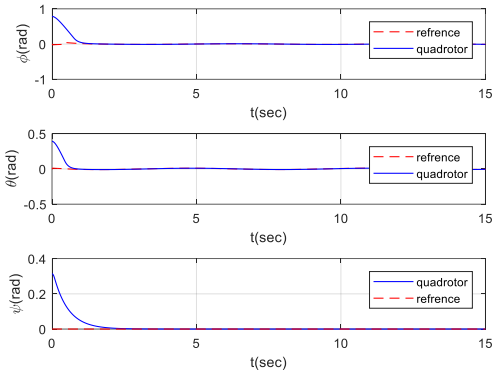

Figure 4. Response curves of attitude for quadrotor

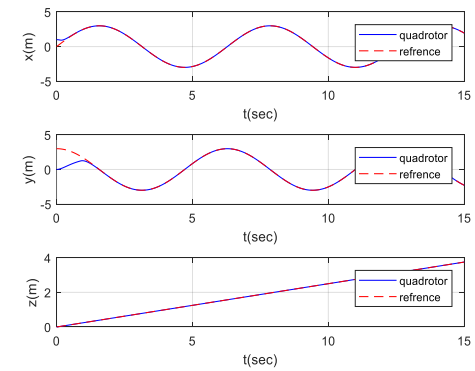

Figure 5. Response curves of position for quadrotor

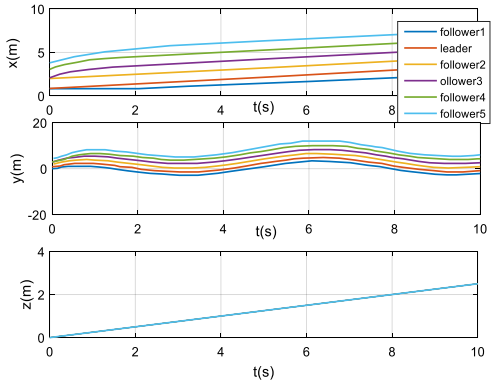

Figure 6. The position of the robots in the S-shaped path

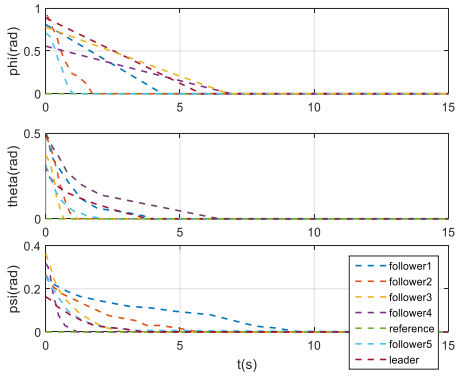

Figure 7. The attitude of the quadrotors in the s-shaped path

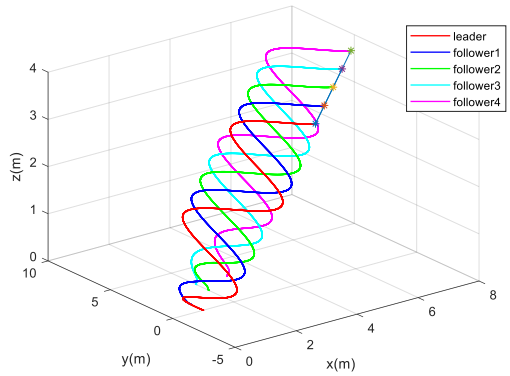

Figure 8. 3D diagram of quadrotors along the s-shaped path

passes through static obstacles. In the second mission, the quadrotors have a square arrangement, and the obstacles are dynamic. In the third mission, the quadrotors have a hexagonal arrangement, and the obstacles are fixed. In this mission, the target is dynamic. In the final mission, the quadrotors have a hexagonal arrangement, and the obstacles are dynamic.

The results of the first mission are given in Figure 9. The quadrotors have passed the static obstacles and have maintained a square formation, and the leader has reached the target. In this figure, the leader is at the point (-3, -43), and after passing the obstacles, she reaches the point (7, 20). Followers are also located at points (-10, 50), (-3, 50) and (-10, -43), and after passing the dynamic obstacles, they are placed in points (-3, 10), (7, 9.5), and (-3, 19.5), which maintain up to 95% accuracy of the square shape after passing the obstacles. The locations of obstacles are shown in Table 2.

In the second mission, four agents were considered. The obstacles are dynamic. The simulation results of this mission are given in Figures 10-12. The velocity of all obstacles is $V = [-3t(i), 9t(i), 12t(i)]$.

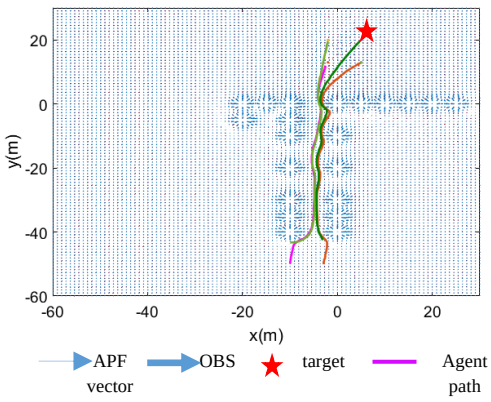

Figure 9. The flight path of the agents in the square arrangement

TABLE 2. Position of obstacles

Obstacle	X(m)	Y(m)	Z(m)
1	-10	-40	15
2	-10	-35	14
3	-10	-30	12
4	-10	-20	15
5	-10	-10	12
6	-10	-5	12
7	-10	0	15
8	-15	0	20
9	-20	0	20
10	-20	-5	18
11	0	-40	25
12	0	-35	15
13	0	-30	15
14	0	-20	20
15	0	-10	20
16	0	0	18
17	5	0	18
18	10	0	15
19	15	0	15
20	20	0	20

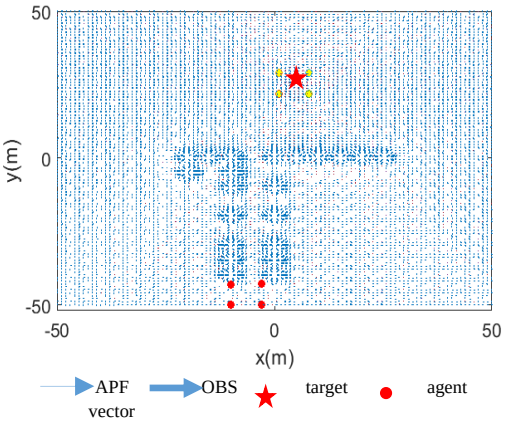

Figure 10. The positions of the agents at the beginning of the flight

Figure 10 indicates the position of the agents at the beginning of the flight, as well as the expected position of the agents after crossing the obstacles.

Figure 11 presents the position of agents while crossing the obstacles.

Figure 12 indicates the position of agents after crossing the obstacles. This figure shows the successful

passing of the agents through the dynamic obstacles and maintaining the square arrangement after crossing. As it is clear from Figures 10, 11, and 12, the leader is at the point (-3, -43) at the beginning of the flight, and after passing the dynamic obstacles, it reaches the point (10, 30). Which is as expected. Followers, who were initially located at points (-10, -50), (-3,50), and (-10, -43), after passing the obstacles, reach points (3, 19.7), (10, 20) and (3, 29.6), which as expected should be at points (3, 20), (10, 20) and (3, 30), and therefore, the simulation with 95% accuracy has kept its square formation and is as expected.

In the third mission, the number of agents has increased to 6. Obstacles are fixed, and the target is moving. The simulations of this mission are presented in Figure 13. The results indicate that the quadrotors passed the obstacles, and the leader tracked the target. According to Figure 13, the leader is at point (40, 32) at the beginning of the flight, and after passing through the obstacles, it reaches point (129, 107), which is expected to reach point (130, 107). Also, the followers are located at points (40, 15), (30, 15), (22, 22), (30, 32), and (47, 22)

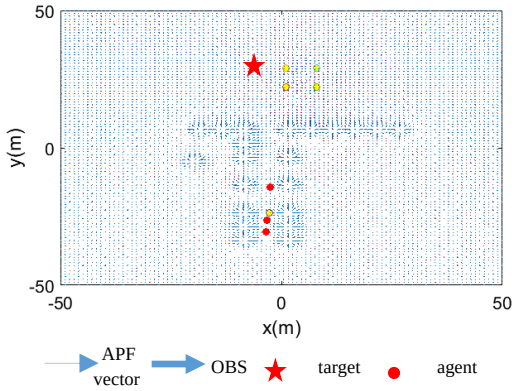

Figure 11. Agents crossing obstacles during flight

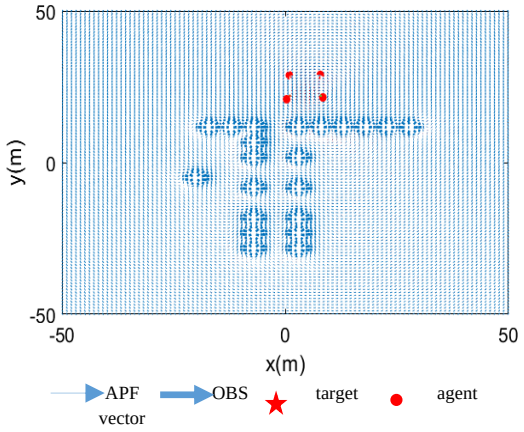

Figure 12. The position of the agents after crossing the obstacles

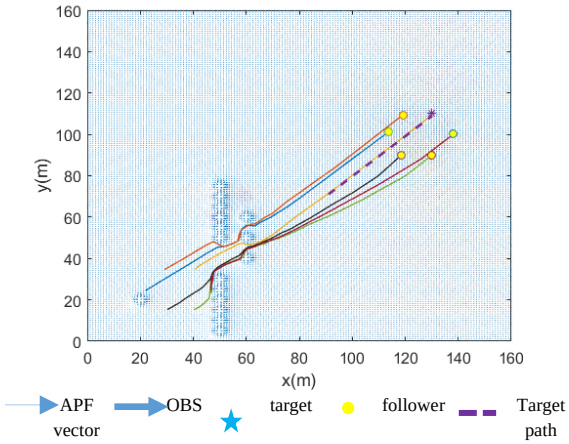

Figure 13. Quadrotors crossing static obstacles

at beginning of the flight, which reach points (130, 90), (120, 91), (112, 98), (120, 107) and (140, 98) after passing the static obstacles. Which, as expected, should be placed in points (130, 90), (120, 90), (112, 97), (120, 107), and (140, 97), respectively. Therefore, the simulations maintain the hexagonal formation with an accuracy of more than 95%. Also, in this mission, the target is moving and is first located at the point (90, 65) and reaches the point (120, 107), which the leader tracks. The location of the obstacles is shown in Table 3.

In the fourth mission, six robots are considered. Obstacles are dynamic, and the target is static. The simulations of this mission are present in Figures 14-16. Figure 14, shows the initial position of the quadrotors and target.

TABLE 3. Obstacles position

Obstacle	X(m)	Y(m)	Z(m)
1	50	5	20
2	50	10	20
3	50	15	20
4	50	16	20
5	50	16	20
6	50	50	22.5
7	50	55	22.5
8	50	60	22.5
9	50	65	22.5
10	50	70	22.5
11	50	75	22.5
12	60	40	22.5
13	50	20	20
14	60	50	22.5
15	60	60	22.5

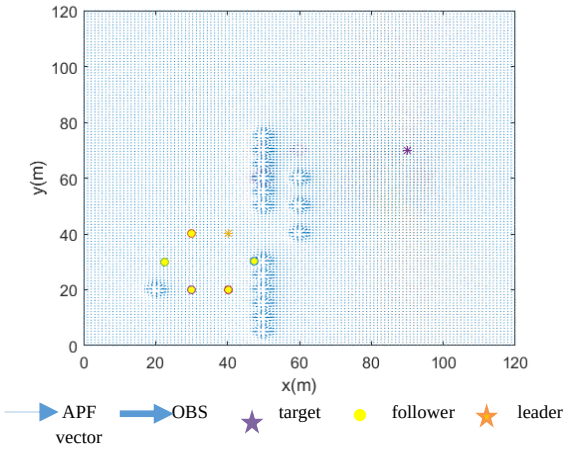

Figure 14. The initial position of quadrotors, obstacles, and targets

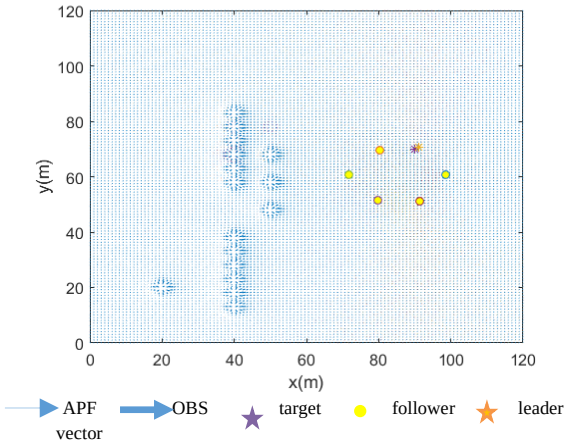

Figure 16. Preserving formation flight after crossing obstacles

Figure 15 indicates that the quadrotors are crossing obstacles, and the leader is moving towards the target.

Figure 16 indicates the quadrotors passing through the moving obstacles and the leader reaching the target. After passing through the obstacles, the quadrotors preserve the hexagonal flight arrangement.

In these figures, it is clear that the leader is initially located at point (40, 40) and reaches point (90, 71) after passing the obstacles. As expected, it should reach the point (90, 70). Other followers are located at the points (40, 20), (30, 20), (20, 30), (30, 40), and (47, 30) at the beginning of the flight, and after passing the dynamic obstacles, they have reached the points (90, 51), (80, 49), (70, 59), (80, 71) and (97, 60) according to Expectations should have reached the points (90, 50), (80, 50), (70, 60), (80, 70) and (97, 60). These results showed that the flight group maintained the hexagonal flight arrangement after crossing the obstacles with 95% accuracy. These results are consistent with crossing the obstacles of reported in literature (36), in which the APF method was used.

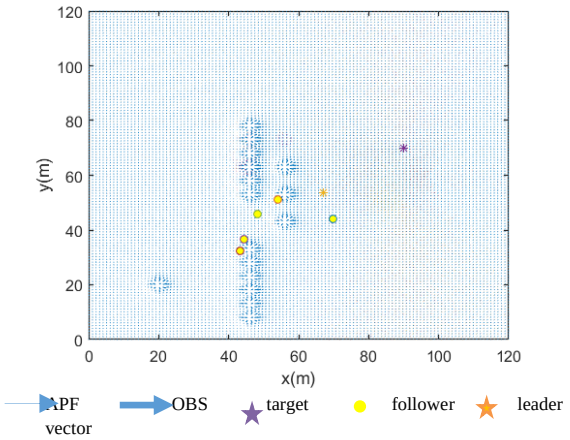

Figure 15. Agents passing through dynamic obstacles

In this section, the simulation results are given. First, the results of controlling the position and condition of the quadrotor are shown. The quadrotors converged to the reference in less than two seconds, and there was no sharp fluctuation in the responses. The results of formation control show that five quadrotors have followed the leader. Finally, the results of avoiding collisions with obstacles on the improved artificial potential field in four missions were presented. In the first mission, four quadrotors were considered, and the obstacles were static. In the second mission, four agents crossed dynamic obstacles. In the third mission, six quadrotors crossed static obstacles, and the target was moving. In the last scenario, six quadrotors crossed dynamic obstacles. The results of these simulations showed that the quadrotors maintained their flight formation after crossing the obstacles with 95% accuracy.

6. CONCLUSION

In this article, quadrotor formation control and obstacle avoidance, and moving target tracking are investigated. To achieve this goal, in the first step, the simulations of the position and attitude controller were presented, which showed that the convergence time of the responses is at most 3 seconds, which is an acceptable time, and severe overshoot and undershoot were not observed. The results of simulation of formation control by the MPC method in an S-shaped path and linear arrangement show that the followers follow the leader and maintain a certain distance and angle from the leader. Obstacle-crossing results using the improved APF were presented in 4 missions. In the first scenario, three quadrotors followed the leader and crossed static obstacles, and maintained a

square formation. In the second scenario, four quadrotors passed dynamic obstacles and, after passing and preserved the square formation. In the third mission, six quadrotors crossed the static obstacles, and the leader tracked the moving target. In the last mission, six quadrotors crossed the dynamic obstacles. In these two missions, the flight group maintained a hexagonal formation after passing through the dynamic and static obstacles. The results of these simulations show the success of the method used to track the moving target and pass the quadrotors through fixed and moving obstacles, by increasing the agents and changing the flight formation. Also, the problem of getting stuck in the local minimum and not passing through environments with many obstacles has not occurred, which indicates the efficiency of the improved APF method.

7. REFERENCES

1. Procter S, Secco EL. Design of a biomimetic BLDC driven robotic arm for teleoperation & biomedical applications. J Hum Earth Future ISSN. 2022:2785-997. 10. 28991/HEF-2021-02-04-03
2. Arofiati F, Sekhar R, Rijalusalam DU. PID-based with Odometry for Trajectory Tracking Control on Four-wheel Omnidirectional Covid-19 Aromatherapy Robot. 2021. 10.28991/esj-2021-SPER-13
3. Doakhan M, Kabganian M, Azimi A. Cooperative payload transportation with real-time formation control of multi-quadrotors in the presence of uncertainty. Journal of the Franklin Institute. 2023;360(2):1284-307. 10.1016/j.jfranklin.2022.11.002
4. Andaluz GM, Leica P, Herrera M, Morales L, Camacho O. Hybrid Controller based on Null Space and Consensus Algorithms for Mobile Robot Formation. Emerging Science Journal. 2022;6(3):429-47. 10.28991/ESJ-2022-06-03-01
5. Chevet T, Vlad C, Maniu CS, Zhang Y. Decentralized MPC for UAVs formation deployment and reconfiguration with multiple outgoing agents. Journal of Intelligent & Robotic Systems. 2020;97:155-70. 10.1007/s10846-019-01025-x
6. Wang X, Xi L, Chen Y, Lai S, Lin F, Chen BM. Decentralized MPC-based trajectory generation for multiple quadrotors in cluttered environments. Guidance, Navigation and Control. 2021;1(02):2150007. 10.1142/S2737480721500072
7. Wang B, Han Y, Wang S, Tian D, Cai M, Liu M, et al. A Review of Intelligent Connected Vehicle Cooperative Driving Development. Mathematics. 2022;10(19):3635. 10.3390/math10193635
8. Zou Y, Meng Z. Coordinated trajectory tracking of multiple vertical take-off and landing UAVs. Automatica. 2019;99:33-40. 10.1016/j.automatica.2018.10.011
9. Dong X, Zhou Y, Ren Z, Zhong Y. Time-varying formation tracking for second-order multi-agent systems subjected to switching topologies with application to quadrotor formation flying. IEEE Transactions on Industrial Electronics. 2016;64(6):5014-24. 10.1109/TIE.2016.2593656
10. Du H, Zhu W, Wen G, Duan Z, Lü J. Distributed formation control of multiple quadrotor aircraft based on nonsmooth consensus algorithms. IEEE transactions on cybernetics. 2017;49(1):342-53. 10.1109/TCYB.2017.2777463
11. Jasim W, Gu D. Robust team formation control for quadrotors. IEEE Transactions on Control Systems Technology. 2017;26(4):1516-23. 10.1109/TCST.2017.2705072
12. Li M, Zhang H, editors. AUV 3D path planning based on A* algorithm. 2020 Chinese Automation Congress (CAC); 2020: IEEE. 10.1109/CAC51589.2020.9327873
13. Yan S, Pan F, editors. Research on route planning of AUV based on genetic algorithms. 2019 IEEE International Conference on Unmanned Systems and Artificial Intelligence (ICUSAI); 2019: IEEE. 10.1109/ICUSAI47366.2019.9124785
14. MahmoudZadeh S, Powers DM, Yazdani AM, Sammut K, Atyabi A. Efficient AUV path planning in time-variant underwater environment using differential evolution algorithm. Journal of Marine Science and Application. 2018;17:585-91. 10.1007/s11804-018-0034-4
15. Che G, Liu L, Yu Z. An improved ant colony optimization algorithm based on particle swarm optimization algorithm for path planning of autonomous underwater vehicle. Journal of Ambient Intelligence and Humanized Computing. 2020;11:3349-54. 10.1007/s12652-019-01531-8
16. Lim HS, Fan S, Chin C, Chai S, Bose N. Particle swarm optimization algorithms with selective differential evolution for AUV path planning. 2020. 10.11591/ijra.v9i2
17. Li X, Wang W, Song J, Liu D, editors. Path planning for autonomous underwater vehicle in presence of moving obstacle based on three inputs fuzzy logic. 2019 4th Asia-Pacific Conference on Intelligent Robot Systems (ACIRS); 2019: IEEE. 10.1109/ACIRS.2019.8936029
18. Sun B, Zhu D, Tian C, Luo C. Complete coverage autonomous underwater vehicles path planning based on glasius bio-inspired neural network algorithm for discrete and centralized programming. IEEE transactions on cognitive and developmental systems. 2018;11(1):73-84. 10.1109/TCDS.2018.2810235
19. Taheri E, Ferdowsi MH, Danesh M. Closed-loop randomized kinodynamic path planning for an autonomous underwater vehicle. Applied Ocean Research. 2019;83:48-64. 10.1016/j.apor.2018.12.008
20. Zhao Y, Hao L-Y, Wu Z-J. Obstacle Avoidance Control of Unmanned Aerial Vehicle with Motor Loss-of-Effectiveness Fault Based on Improved Artificial Potential Field. Sustainability. 2023;15(3):2368. 10.3390/su15032368
21. Shang W, Jing G, Zhang D, Chen T, Liang Q. Adaptive fixed time nonsingular terminal sliding-mode control for quadrotor formation with obstacle and inter-quadrotor avoidance. IEEE Access. 2021;9:60640-57. 10.1109/ACCESS.2021.3074316
22. Pan Z, Li D, Yang K, Deng H. Multi-robot obstacle avoidance based on the improved artificial potential field and PID adaptive tracking control algorithm. Robotica. 2019;37(11):1883-903. 10.1017/S026357471900033X
23. Wang X, Zhang J, editors. Path Planning of Load Transportation by Multi-Quadrotor Formation Based on RRT-APF Method. 2022 5th International Conference on Robotics, Control and Automation Engineering (RCAE); 2022: IEEE. : 10.1109/RCAE56054.2022.9995950
24. Qiao Y, Huang X, Yang B, Geng F, Wang B, Hao M, et al. Formation Tracking Control for Multi-Agent Systems with Collision Avoidance and Connectivity Maintenance. Drones. 2022;6(12):419. 10.3390/drones6120419
25. Aljassani AM, Ghani SN, Al-Hajjar AM. Enhanced multi-agent systems formation and obstacle avoidance (EMAFOA) control algorithm. Results in Engineering. 2023;18:101151. 10.1016/j.rineng.2023.101151
26. Huang Y, Liu W, Li B, Yang Y, Xiao B. Finite-time formation tracking control with collision avoidance for quadrotor UAVs.

Journal of the Franklin Institute. 2020;357(7):4034-58. 10.1016/j.jfranklin.2020.01.014

27. Zhang J, Xie F, Yin D, Qi Y, Luo D, editors. Formation Control and Obstacle Avoidance for UAV Group. International Conference on Autonomous Unmanned Systems; 2021: Springer. 10.1007/978-981-16-9492-9_77
28. Ge SS, Cui YJ. Dynamic motion planning for mobile robots using potential field method. Autonomous robots. 2002;13:207-22. 10.1023/A:1020564024509
29. Li Q, Wang L, Chen B, Zhou Z, editors. An improved artificial potential field method for solving local minimum problem. 2011 2nd International Conference on Intelligent Control and Information Processing; 2011: IEEE. 10.1109/ICICIP.2011.6008278
30. Abdellatif RA, El-Badawy AA, editors. Artificial potential field for dynamic obstacle avoidance with mpc-based trajectory tracking for multiple quadrotors. 2020 2nd novel intelligent and leading emerging sciences conference (NILES); 2020: IEEE. 10.1109/NILES50944.2020.9257973
31. Du Y, Zhang X, Nie Z. A real-time collision avoidance strategy in dynamic airspace based on dynamic artificial potential field algorithm. IEEE Access. 2019;7:169469-79. 10.1109/ACCESS.2019.2953946
32. Ghaderi F, Toloei A, Ghasemi R. Formation control of unmanned helicopters using the sliding mode controller method. Technology in Aerospace Engineering. 2023:1-11. 10.22034/jtae.2023.359555.1263
33. Kuriki Y, Namerikawa T. Formation control with collision avoidance for a multi-UAV system using decentralized MPC and consensus-based control. SICE Journal of Control, Measurement, and System Integration. 2015;8(4):285-94. 10.9746/jcmsi.8.285
34. Joelianto E, Maryami Sumarjono E, Budiyono A, Retnaning Penggalih D. Model predictive control for autonomous unmanned helicopters. Aircraft Engineering and Aerospace Technology. 2011;83(6):375-87. 10.1108/00022661111173252
35. Du H, Zhu W, Wen G, Wu D. Finite-time formation control for a group of quadrotor aircraft. Aerospace Science and Technology. 2017;69:609-16. 10.1016/j.ast.2017.07.012
36. Ma'Arif A, Rahmaniar W, Vera MAM, Nuryono AA, Majdoubi R, Çakan A, editors. Artificial potential field algorithm for obstacle avoidance in uav quadrotor for dynamic environment. 2021 IEEE International Conference on Communication, Networks and Satellite (COMNETSAT); 2021: IEEE. 10.1109/COMNETSAT53002.2021.9530803

Persian Abstract

چکیده

هدف از این مقاله کنترل شکل‌دهی و عبور از موانع ایستا و دینامیک برای گروه کوادروتور، حفظ تداوم و آرایش پرواز پس از عبور از موانع و ردیابی هدف متحرک است. برای کنترل وضعیت و موقعیت کوادروتورها و کنترل شکل‌دهی از روش MPC استفاده شده است. شکل گیری پرواز بر اساس روش پیرو-پیشرو است که در آن پیروان با استفاده از کنترل کننده شکل‌دهی، زاویه و فاصله مشخصی را از پیشرو حفظ می کنند. روش APF بهبود یافته برای عبور از موانع استفاده شده است که مزیت اصلی آن در مقایسه با APF سنتی افزایش برد نیروی دافعه موانع است که مشکل گیر افتادن در حداقل محلی و عدم عبور در محیط‌های پرمانع را حل می‌کند. نتایج طراحی کنترل کننده وضعیت و موقعیت نشان داد که کوادروتورها در کمتر از سه ثانیه همگرا شدند. شبیه سازی‌های کنترل شکل‌دهی در مسیر مارپیچی نشان داد که پیروان، از رهبر پیروی می‌کنند. نتایج عبور کوادروتورها از موانع در چهار ماموریت ارائه شد. در ماموریت اول چهار کوادروتور از موانع ساکن عبور کردند. در ماموریت دوم چهار کوادروتور از موانع دینامیکی عبور کردند. در این دو ماموریت، کوادروتورها پس از عبور از موانع، ساختار پروازی مربعی را حفظ کردند. در ماموریت سوم تعداد کوادروتورها به شش نفر افزایش یافت.لیدر هدف متحرک را ردیابی کرد و کوادروتورها از موانع ساکن عبور کردند. در آخرین ماموریت، کوادروتورها از موانع دینامیکی عبور کردند و لیدر هدف ثابت را ردیابی کرد. در این ماموریت ها، کوادروتورها پس از عبور از موانع، آرایش شش ضلعی را حفظ می کنند. شبیه سازی نتایج نشان داد که کوادروتورها از موانع ثابت و متحرک عبور کرده و پس از عبور، آرایش پرواز را حفظ کردند.